

PREPARED FOR THE U.S. DEPARTMENT OF ENERGY,
UNDER CONTRACT DE-AC02-76CH03073

PPPL-3691
UC-70

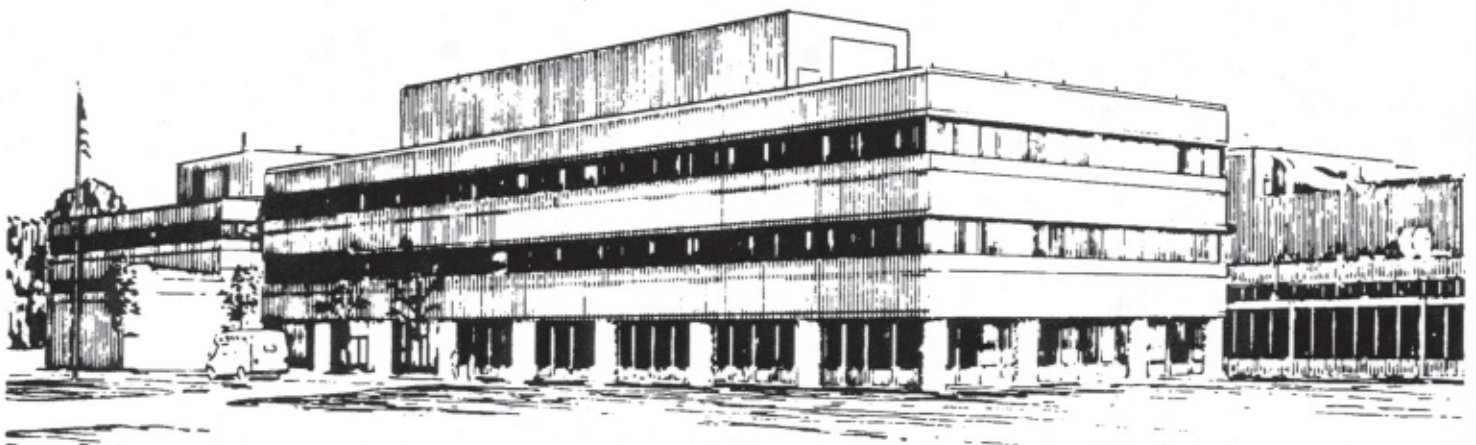
PPPL-3691

**Nonlinear δf Simulation Studies of Intense Charged
Particle Beams with Large Temperature Anisotropy**

by

Edward A. Startsev, Ronald C. Davidson, and Hong Qin

May 2002



**PRINCETON PLASMA PHYSICS LABORATORY
PRINCETON UNIVERSITY, PRINCETON, NEW JERSEY**

PPPL Reports Disclaimer

This report was prepared as an account of work sponsored by an agency of the United States Government. Neither the United States Government nor any agency thereof, nor any of their employees, makes any warranty, express or implied, or assumes any legal liability or responsibility for the accuracy, completeness, or usefulness of any information, apparatus, product, or process disclosed, or represents that its use would not infringe privately owned rights. Reference herein to any specific commercial product, process, or service by trade name, trademark, manufacturer, or otherwise, does not necessarily constitute or imply its endorsement, recommendation, or favoring by the United States Government or any agency thereof. The views and opinions of authors expressed herein do not necessarily state or reflect those of the United States Government or any agency thereof.

Availability

This report is posted on the U.S. Department of Energy's Princeton Plasma Physics Laboratory Publications and Reports web site in Fiscal Year 2002. The home page for PPPL Reports and Publications is: http://www.pppl.gov/pub_report/

DOE and DOE Contractors can obtain copies of this report from:

U.S. Department of Energy
Office of Scientific and Technical Information
DOE Technical Information Services (DTIS)
P.O. Box 62
Oak Ridge, TN 37831

Telephone: (865) 576-8401
Fax: (865) 576-5728
Email: reports@adonis.osti.gov

This report is available to the general public from:

National Technical Information Service
U.S. Department of Commerce
5285 Port Royal Road
Springfield, VA 22161

Telephone: 1-800-553-6847 or
(703) 605-6000
Fax: (703) 321-8547
Internet: <http://www.ntis.gov/ordering.htm>

Nonlinear δf simulation studies of intense charged particle beams with large temperature anisotropy

Edward A. Startsev, Ronald C. Davidson and Hong Qin

Plasma Physics Laboratory, Princeton University, Princeton, NJ 08543

Abstract

In this paper, a 3D nonlinear perturbative particle simulation code (BEST) [H. Qin, R. C. Davidson and W. W. Lee, Physical Review Special Topics on Accelerators and Beams **3**, 084401 (2000)] is used to systematically study the stability properties of intense nonneutral charged particle beams with large temperature anisotropy ($T_{\perp b} \gg T_{\parallel b}$). The most unstable modes are identified, and their eigenfrequencies, radial mode structure, and nonlinear dynamics are determined for axisymmetric perturbations with $\partial/\partial\theta = 0$.

I. INTRODUCTION

Periodic focusing accelerators, transport systems and storage rings [1–5] have a wide range of applications ranging from basic scientific research in high energy and nuclear physics, to applications such as heavy ion fusion, spallation neutron sources, tritium production and nuclear waste transmutation, to mention a few examples. Of particular importance at the high beam currents and charge densities of practical interest, are the effects of the intense self fields produced by the beam space charge and current on determining the detailed equilibrium, stability and transport properties. While considerable progress has been made in understanding the self-consistent evolution of the beam distribution function, $f_b(\mathbf{x}, \mathbf{p}, t)$, and self-generated electric and magnetic fields, $\mathbf{E}^s(\mathbf{x}, t)$ and $\mathbf{B}^s(\mathbf{x}, t)$, in kinetic analyses based on the nonlinear Vlasov-Maxwell equations [1, 6–10], in numerical simulation studies of intense beam propagation [11–19], and in macroscopic warm-fluid models [20–23], the effects of finite geometry and space-charge effects often make predictions of detailed stability behavior difficult. It is therefore important to develop an improved understanding of fundamental collective stability properties, including the case where a large temperature anisotropy ($T_{\perp b} \gg T_{\parallel b}$) can drive a Harris-like instability [24, 25], familiar in the study of electrically neutral plasmas.

It's well known that in neutral plasmas with strongly anisotropic distributions ($T_{\parallel b}/T_{\perp b} \ll 1$) a collective instability may develop if there is sufficient coupling between the transverse and longitudinal degrees of freedom [24, 25]. Such anisotropies develop naturally in accelerators, where the longitudinal temperature of the accelerated beam of charged particles with charge q accelerated by a voltage V is reduced according to $T_{\parallel bf} = T_{\parallel bi}^2/2qV$ (for a nonrelativistic beam). At the same time, the transverse temperature may increase due to nonlinearities in the applied and self-field forces, nonstationary beam profiles, and beam mismatch. These processes provide the free energy to drive collective instabilities and may lead to a deterioration of beam quality [18, 26, 27]. Historically, this instability was first studied analytically by Wang and Smith [8] for beams with a Kapchinkij – Vladimirskij (KV) distribution. Friedman, et. al. [29–31] reported a rapid 'equilibration' process observed in 3D particle simulations of KV beams with large temperature anisotropy using the WARP code. They conjectured that the initial rapid heating in the longitudinal direction may be the result of an anisotropy-driven instability reminiscent of a Harris mode, but with

transverse betatron motion instead of cyclotron motion. Realizing the fact that the highly inverted KV distribution may introduce numerous unstable modes, Lund, et. al. [32, 33] used a semi-gaussian distribution to carry out particle-in-cell simulations of the instability. However, unlike the KV distribution, the semi-gaussian distribution is not a rigorous equilibrium solution of the Vlasov-Maxwell equations. The departure from a self-consistent equilibrium inevitably leads to mode excitations which can be confused with those due the anisotropy-driven instability. The bi-Maxwellian distribution considered in the present study is a rigorous steady-state equilibrium of the Vlasov-Maxwell equations, and it does not support the spurious modes of the KV distribution. In addition, the bi-Maxwellian distribution is known to be a stable equilibrium with respect to transverse perturbations [9], and therefore is an ideal candidate for studying instabilities driven by temperature anisotropy. A simple theory of the instability for a bi-Maxwellian distribution is presented in this paper, which appears to capture its main features and is a relatively straightforward generalization of the analysis of the Harris instability to the case of an intense particle beam. In this paper, we present the instability thresholds obtained in the simulations, as well as detailed simulations of the nonlinear development and saturation of the instability. We identify the main saturation mechanism as quasilinear stabilization due to resonant wave-particle interaction (Landau damping). A 3D nonlinear perturbative particle simulation code [14–16], called the Beam Equilibrium, Stability and Transport (BEST) code, is used to systematically study the electrostatic stability properties of intense nonneutral charged particle beams with large temperature anisotropy ($T_{\perp b} \gg T_{\parallel b}$). The most unstable modes are identified, and their eigenfrequencies, radial mode structure, and nonlinear dynamics are determined for axisymmetric perturbations with $\partial/\partial\theta = 0$. Since a well-behaved bi-Maxwellian distribution is used in the simulations, the mode structures observed are different from those of the KV distribution previously reported.

The organization of this paper is the following. In Sec. II, we present a simple kinetic model of the instability based on a matrix dispersion equation derived from the linearized Vlasov-Poisson equations. The nonlinear δf simulation method is briefly described in Sec. III, and in Sec. IV we present detailed simulation results for a wide range of system parameters.

II. LINEAR STABILITY THEORY

A. Kinetic Description

Wang and Smith [8] investigated the kinetic stability properties of an intense particle beam assuming a Kapchinkij-Vladimirskij (KV) beam distribution [6] in the limit of large energy anisotropy ($T_{\parallel b}/T_{\perp b} \rightarrow 0$) by expanding the solution of the linearized Vlasov-Poisson equations in a series of Gluckstern eigenfunctions $\delta\varphi_n(r) = (1/2)[P_{n-1}(1 - 2r^2/r_b^2) + P_n(1 - 2r^2/r_b^2)]$, where $P_n(x)$ is the n 'th-order Legendre polynomial [7]. The expansion yields a dispersion relation, expressible in terms of an infinite matrix determinant. For long-wavelength axial perturbations with $k_z^2 r_b^2 \ll 1$, one-half of the modes [8] are identified as transverse (T_n) Gluckstern modes with eigenfunction $\delta\varphi \propto \delta\varphi_n$. The other half [8] consists of modes corresponding in the limit of large tune depression ($\nu \rightarrow 0$) to an ordinary cold-beam longitudinal mode (L_1) with eigenfunction $\delta\varphi \propto J_0(k_z r)$ inside the beam and dispersion relation $(\omega - k_z V_b)^2 = (\hat{\omega}_{pb}^2/2)(k_z r_b)^2 \ln(r_w/r_b)$, plus a less-known class of ‘‘coupling’’ modes (L_n) with $\delta\varphi \propto \delta\varphi_n$ and $(\omega - k_z V_b)^2 = [\hat{\omega}_{pb}^2/8n(n+1)](k_z r_b)^2 \int_0^{2\pi} (dx/2\pi) P_n(\cos x)$. The latter modes are the result of the interaction between transversely oscillating particles and the longitudinal perturbed potential. Here, ω is the mode oscillation frequency, k_z is the axial wavenumber of the perturbation, $V_b = \beta c$ is the axial beam velocity, and $J_0(x)$ is the ordinary Bessel function of the first kind of the order zero. Furthermore, $\nu = \nu_0(1 - s_b)^{1/2}$ is the depressed tune, where $s_b = \hat{\omega}_{pb}^2/2\gamma_b^2\omega_f^2$ is the normalized beam intensity, $\hat{\omega}_{pb}^2 = 4\pi\hat{n}_b e_b^2/\gamma_b m_b$ is the relativistic plasma frequency-squared, $\nu_0 = \omega_f$ is the transverse betatron frequency associated with the applied focusing field, r_b is the beam edge radius, r_w is the radius of the perfectly conducting wall, $\gamma_b = (1 - \beta_b^2)^{-1/2}$ is the relativistic mass factor, e_b and m_b are the particle charge and rest mass, respectively, and \hat{n}_b is the number density of the beam particles.

As a general rule, for a KV distribution, instability arises in the regions of parameter space where two or more modes interact resonantly. The transverse modes (T_n) are not significantly affected by longitudinal perturbations, and therefore the instability due to their interaction is a consequence of the fact that the KV distribution has a highly inverted population in phase space [1, 6–8]. The most dangerous $T_n - L_k$ instabilities are due to $T_2 - L_1$ interactions [8] in the region where $\nu/\nu_0 \simeq 0.44$ with maximum growth rate $Im\omega/\nu_0 \simeq 0.03$, and due to $T_2 - L_2$

interactions in the region $0.2 \leq \nu/\nu_0 \leq 0.32$, with maximum growth rate $Im\omega/\nu_0 \simeq 0.15$. The latter mode has a much higher growth rate due to the similar transverse structure of the L_2 and T_2 modes. The growth rate obtained by Wang and Smith [8] is a maximum for $k_z^2 r_b^2 \gtrsim 1$ in both cases.

It is important to extend theoretical studies of the kinetic stability properties of anisotropic beams to distribution functions other than the KV distribution. This is because the KV distribution has an (unphysical) inverted population in transverse phase-space variables, which provides the free energy to drive collective instabilities at high beam intensities that are intrinsic to this inverted population [7, 8]. This, of course, can mask the effects of anisotropy-driven instabilities. To this end, we briefly outline here a simple derivation of the Harris-like instability [24, 25] in intense particle beams for electrostatic perturbations about the thermal equilibrium distribution with temperature anisotropy ($T_{\perp b} > T_{\parallel b}$) described in the beam frame by the self-consistent axisymmetric Vlasov equilibrium [1, 10]

$$f_b^0(r, \mathbf{p}) = \frac{\hat{n}_b}{(2\pi m_b T_{\perp b})} \exp\left(-\frac{H_{\perp}}{T_{\perp b}}\right) \frac{1}{(2\pi m_b T_{\parallel b})^{1/2}} \exp\left(-\frac{p_z^2}{2m_b T_{\parallel b}}\right). \quad (1)$$

Here, $H_{\perp} = p_{\perp}^2/2m_b + (1/2)m_b\omega_f^2(x^2 + y^2) + e_b\phi^0(r)$ is the single-particle Hamiltonian, $p_{\perp} = (p_x^2 + p_y^2)^{1/2}$ is the transverse particle momentum, $r = (x^2 + y^2)^{1/2}$ is the radial distance from the beam axis, $\omega_f = const.$ is the transverse frequency associated with the applied focusing field, and $\phi^0(r)$ is the equilibrium space-charge potential determined self-consistently from Poisson's equation, $r^{-1}(\partial/\partial r)(r\partial\phi^0/\partial r) = -4\pi e_b n_b^0$, where $n_b^0(r) = \int d^3p f_b^0(r, \mathbf{p})$ is the equilibrium number density of beam particles. For simplicity, the analysis is carried out in the beam frame ($V_b = 0$ and $\gamma_b = 1$). Furthermore, setting $\phi^0(r=0) = 0$, the constant \hat{n}_b occurring in Eq. (1) can be identified with the on-axis density $n_b^0(r=0)$, and the constants $T_{\perp b}$ and $T_{\parallel b}$ can be identified with the transverse and longitudinal temperatures (energy units), respectively.

For present purposes, we consider small-amplitude, axisymmetric ($\partial/\partial\theta = 0$) electrostatic perturbations of the form

$$\delta\phi(\mathbf{x}, t) = \widehat{\delta\phi}(r) \exp(ik_z z - i\omega t), \quad (2)$$

where $\delta\phi(\mathbf{x}, t)$ is the perturbed electrostatic potential, k_z is the axial wavenumber, and ω is the complex oscillation frequency, with $Im\omega > 0$ corresponding to instability (temporal growth). Without presenting algebraic details, using the method of characteristics, the

linearized Poisson equation can be expressed as

$$\frac{1}{r} \frac{\partial}{\partial r} r \frac{\partial}{\partial r} \widehat{\delta\phi}(r) - k_z^2 \widehat{\delta\phi}(r) = -4\pi e_b \int d^3 p \widehat{\delta f_b}(r, \mathbf{p}), \quad (3)$$

where

$$\begin{aligned} \widehat{\delta f_b}(r, \mathbf{p}) = & -\frac{e_b}{T_{\perp b}} \widehat{\delta\phi} f_b^0 - \frac{e_b}{T_{\perp b}} \left[\omega - k_z v_z \left(1 - \frac{T_{\perp b}}{T_{\parallel b}} \right) \right] f_b^0 \\ & \times i \int_{-\infty}^t dt' \widehat{\delta\phi}[r'(t')] \exp[i(k_z v_z - \omega)(t' - t)] \end{aligned} \quad (4)$$

for perturbations about the choice of the anisotropic thermal equilibrium distribution function in Eq. (1). In the orbit integral in Eq. (4), $Im\omega > 0$ is assumed, and $r'(t') = [x'^2(t') + y'^2(t')]^{1/2}$ is the radial orbit in the equilibrium field configuration such that $[\mathbf{x}'_{\perp}(t'), \mathbf{p}'_{\perp}(t')]$ passes through the phasespace point $(\mathbf{x}_{\perp}, \mathbf{p}_{\perp})$ at time $t' = t$. We express the perturbation amplitude as $\widehat{\delta\phi}(r) = \sum_n \alpha_n \phi_n(r)$, where $\{\alpha_n\}$ are constants, and the complete set of vacuum eigenfunctions $\{\phi_n(r)\}$ is defined by $\phi_n(r) = A_n J_0(\lambda_n r/r_w)$. Here, λ_n is the n 'th zero of $J_0(\lambda_n) = 0$, and $A_n = \sqrt{2}/[r_w J_1(\lambda_n)]$ is a normalization constant such that $\int_0^{r_w} dr r \phi_n(r) \phi_{n'}(r) = \delta_{n,n'}$. We substitute $\widehat{\delta\phi}(r) = \sum_n \alpha_n \phi_n(r)$ into Poisson's equation (3) and operate with $\int_0^{r_w} dr r \phi_{n'}(r) \dots$. This gives the matrix dispersion equation

$$\sum_n \alpha_n D_{n,n'}(\omega) = 0, \quad (5)$$

where

$$D_{n,n'}(\omega) = (\lambda_n^2 + k_z^2 r_w^2) \delta_{n,n'} + \chi_{n,n'}(\omega), \quad (6)$$

and the beam-induced susceptibility $\chi_{n,n'}(\omega)$ is defined by

$$\chi_{n,n'}(\omega) = -4\pi e_b r_w^2 \int_0^{r_w} dr r \phi_{n'}(r) \int d^3 p \widehat{\delta f_b^n}(r, \mathbf{p}). \quad (7)$$

Here, $\widehat{\delta f_b^n}(r, \mathbf{p})$ is defined in Eq. (4) with $\widehat{\delta\phi} \rightarrow \phi_n$. The condition for a nontrivial solution to Eq. (5) is

$$\det\{D_{n,n'}(\omega)\} = 0, \quad (8)$$

which plays the role of a matrix dispersion relation that determines the complex oscillation frequency ω .

We defer a detailed analysis of Eqs.(5)-(8) to a separate paper, and summarize here some *qualitative* properties of the Harris-like instability that ensues in the limit of an anisotropic

beam distribution that is *cold* in the longitudinal direction, i.e.,

$$\frac{T_{\parallel b}}{T_{\perp b}} \rightarrow 0. \quad (9)$$

In this regard, it is convenient to introduce the effective *depressed* betatron frequency $\omega_{\beta\perp}$. It can be shown [1] that for the equilibrium distribution in Eq. (1), the mean-square beam radius r_b^2 defined by

$$r_b^2 = \langle r^2 \rangle = \frac{\int dr r^3 n_b^0(r)}{\int dr r n_b^0(r)}, \quad (10)$$

is related exactly to the line density $N_b = 2\pi \int dr r n_b^0(r)$, and transverse beam temperature $T_{\perp b}$ by the equilibrium radial force balance equation [1]

$$\omega_f^2 r_b^2 = \frac{N_b e_b^2}{m_b} + \frac{2T_{\perp b}}{m_b}. \quad (11)$$

Equation (11) can be rewritten as

$$\left(\omega_f^2 - \frac{1}{2} \bar{\omega}_{pb}^2 \right) r_b^2 = \frac{2T_{\perp b}}{m_b}, \quad (12)$$

where we have introduced the effective *average* beam plasma frequency $\bar{\omega}_{pb}$ defined by

$$r_b^2 \bar{\omega}_{pb}^2 \equiv \int_0^{r_w} dr r \omega_{pb}^2(r) = \frac{2e_b^2 N_b}{m_b}. \quad (13)$$

Then, Eq. (12) can be used to introduce the effective *depressed* betatron frequency $\omega_{\beta\perp}$ defined by

$$\omega_{\beta\perp}^2 \equiv \left(\omega_f^2 - \frac{1}{2} \bar{\omega}_{pb}^2 \right) = \frac{2T_{\perp b}}{m_b r_b^2}. \quad (14)$$

If, for example, the beam density were uniform over the beam cross-section, then Eq. (14) corresponds to the usual definition of the depressed betatron frequency for a KV beam, and it's readily shown that the radial orbit $r'(t')$ occuring in Eqs.(4) and (7) can be expressed as [1]

$$r'^2(t') = r^2 \cos^2(\omega_{\beta\perp} \tau) + \frac{p_{\perp}^2}{m_b^2 \omega_{\beta\perp}^2} \sin^2(\omega_{\beta\perp} \tau) + \frac{r p_{\perp}}{m_b \omega_{\beta\perp}} \cos(\phi - \theta) \sin(2\omega_{\beta\perp} \tau). \quad (15)$$

Here $\tau = t' - t$ is the displaced time variable, and we have expressed $(x, y) = (r \cos \theta, r \sin \theta)$ and $(p_x, p_y) = (p_{\perp} \cos \phi, p_{\perp} \sin \phi)$ in cylindrical polar coordinates. Note from Eq. (15) that $r'(t' = t) = r$ and $[dr'^2/dt']_{t=t'} = 2(xp_x + yp_y)/m_b$, as expected. Due to the nontrivial dependence of the perturbed potential in Eq. (4) on radius r , the transverse betatron motion [Eq. (15)] will drive density perturbations resonantly at frequencies that are multiples of

$2\omega_{\beta\perp}$. Instability occurs when one of these frequencies is close to the beam plasma frequency ω_{pb} .

In general, for the choice of equilibrium distribution function in Eq. (1), there will be a spread in transverse depressed betatron frequencies $\omega_{\beta\perp}(H_{\perp})$, and the particle trajectories will not be described by the simple trigonometric function in Eq. (15). For present purposes, however, we consider a simple *model* in which the radial orbit $r'(t')$ occurring in Eq. (4) and the definition of $\chi_{n,n'}(\omega)$ in Eq. (7) is approximated by Eq. (15) with the constant value $\omega_{\beta\perp}$ defined in Eq. (14) and the *approximate* equilibrium density profile defined by $n_b^0(r) = \hat{n}_b \exp(-m_b \omega_{\beta\perp}^2 r^2 / 2T_{\perp b})$. For a nonuniform beam, $\omega_{\beta\perp}^{-1}$ is the characteristic time for a particle with thermal speed $v_{th\perp} = (2T_{\perp b}/m_b)^{1/2}$ to cross the rms radius r_b of the beam. In this case, $\chi_{n,n'}(\omega)$ can be evaluated in closed analytical form provided the conducting wall is sufficiently far removed from the beam ($r_w/r_b \gtrsim 3$, say). In this case, the matrix elements decrease exponentially away from the diagonal, with

$$\left| \frac{D_{n,n+k}}{D_{n,n}} \right| \sim \exp\left(-\frac{\pi^2 k^2}{4} \frac{r_b^2}{r_w^2}\right), \quad (16)$$

where k is an integer, and we have used the approximate relation $\lambda_n \approx \pi(4n-1)/4$. Therefore, for $r_w/r_b \gtrsim 3$, we can approximate $\{D_{n,n'}(\omega)\}$ by a *tri-diagonal* matrix. In this case, for the lowest-order radial modes ($n=1$ and $n=2$), the matrix dispersion relation (8) can be approximated by

$$D_{1,1}(\omega)D_{2,2}(\omega) - [D_{1,2}(\omega)]^2 = 0, \quad (17)$$

where use has been made of $D_{1,2}(\omega) = D_{2,1}(\omega)$.

We introduce the effective perpendicular thermal speed-squared of a beam particle defined by $v_{th\perp}^2 = 2T_{\perp b}/m_b$. Then, for $T_{\parallel b}/T_{\perp b} \rightarrow 0$ and $r_w/r_b \gtrsim 3$, the approximate dispersion relation (17) describing the coupling of the lowest order $n=1$ mode with the $n=2$ radial mode, within the context of the present simplified model, can be expressed as

$$\begin{aligned} & \left\{ \lambda_1^2 + k_z^2 r_w^2 + \frac{2 \exp(-\frac{k_1^2}{2})(\hat{\omega}_p^2/\omega_{\beta\perp}^2)}{J_1^2(\lambda_1)} \left[I_0\left(\frac{k_1^2}{2}\right) - \left(1 + \frac{k_z^2 v_{th\perp}^2}{2\omega^2}\right) I_0^2\left(\frac{k_1^2}{4}\right) \right. \right. \\ & \quad \left. \left. - \left(\frac{\omega}{\omega - 2\omega_{\beta\perp}} + \frac{k_z^2 v_{th\perp}^2}{2(\omega - 2\omega_{\beta\perp})^2}\right) I_1^2\left(\frac{k_1^2}{4}\right) \right] \right\} \\ & \times \left\{ \lambda_2^2 + k_z^2 r_w^2 + \frac{2 \exp(-\frac{k_2^2}{2})(\hat{\omega}_p^2/\omega_{\beta\perp}^2)}{J_1^2(\lambda_2)} \left[I_0\left(\frac{k_2^2}{2}\right) - \left(1 + \frac{k_z^2 v_{th\perp}^2}{2\omega^2}\right) I_0^2\left(\frac{k_2^2}{4}\right) \right. \right. \\ & \quad \left. \left. - \left(\frac{\omega}{\omega - 2\omega_{\beta\perp}} + \frac{k_z^2 v_{th\perp}^2}{2(\omega - 2\omega_{\beta\perp})^2}\right) I_1^2\left(\frac{k_2^2}{4}\right) \right] \right\} \end{aligned}$$

$$= \frac{(2\hat{\omega}_p^2/\omega_{\beta\perp}^2)^2}{J_1^2(\lambda_1)J_1^2(\lambda_2)} \exp\left(-\frac{(k_1^2 + k_2^2)}{2}\right) \left\{ I_0\left(\frac{k_1 k_2}{2}\right) - \left(1 + \frac{k_z^2 v_{th\perp}^2}{2\omega^2}\right) I_0^2\left(\frac{k_1 k_2}{4}\right) - \left(\frac{\omega}{\omega - 2\omega_{\beta\perp}} + \frac{k_z^2 v_{th\perp}^2}{2(\omega - 2\omega_{\beta\perp})^2}\right) I_1^2\left(\frac{k_1 k_2}{4}\right) \right\}^2, \quad (18)$$

where we have retained only the leading-order nonresonant terms and one resonant term at (positive) frequency $\omega \approx 2\omega_{\beta\perp}$. In the dispersion relation (18), $\lambda_1 \simeq 2.405$ and $\lambda_2 \simeq 5.52$ are determined from the zeros of $J_0(\lambda_n) = 0$, $v_{th\perp} = (2T_{\perp b}/m_b)^{1/2}$ is the transverse thermal speed, k_1 and k_2 are defined by $k_1 = \lambda_1 r_b/r_w$ and $k_2 = \lambda_2 r_b/r_w$, and $\omega_{\beta\perp} = \omega_f(1 - \bar{s}_b)^{1/2}$ is the effective depressed betatron frequency [Eq. (14)], where $\bar{s}_b = \bar{\omega}_{pb}^2/2\omega_f^2$ is the effective normalized beam intensity defined in terms of $\bar{\omega}_{pb}$.

The dispersion relation (18) can be used to investigate detailed electrostatic stability properties for strong anisotropy ($T_{\parallel b}/T_{\perp b} \rightarrow 0$) for a wide range of normalized axial wavenumbers ($k_z r_w$) and effective normalized beam intensity $\bar{s}_b = \bar{\omega}_{pb}^2/2\omega_f^2$, or equivalently, normalized tune depression $\bar{\nu}/\nu_0$ defined by

$$\frac{\bar{\nu}}{\nu_0} \equiv \frac{\omega_{\beta\perp}}{\omega_f} = (1 - \bar{s}_b)^{1/2}. \quad (19)$$

For sufficiently large $k_z r_w$, the large temperature anisotropy ($T_{\parallel b}/T_{\perp b} \rightarrow 0$) in Eq. (18) provides the free energy to drive the classical Harris-type instability [24, 25], generalized here to include finite transverse geometry and beam space-charge effects. The influence of the finite longitudinal temperature can be taken into account if one assumes $T_{\parallel b} \neq 0$ in Eq. (1). This results in the (collisionless) Landau damping of the unstable mode due to resonant wave-particle interactions [1] associated with the axial momentum spread of the beam particles.

To compare with the simulation results in Sec. IV, we introduce the normalized beam intensity s_b defined in terms of the on-axis ($r = 0$) beam density \hat{n}_b . Here, $s_b \equiv \hat{\omega}_{pb}^2/2\omega_f^2$, where $\hat{\omega}_{pb} = (4\pi e_b^2 \hat{n}_b/m_b)^{1/2}$. Using Eqs.(11)-(14), the normalized beam intensity $\bar{s}_b = \bar{\omega}_{pb}^2/2\omega_f^2$ introduced in Eq. (19) is related to s_b by the equation

$$s_b = \bar{s}_b \hat{n}_b \left(\int_0^{r_w} dr r^3 n_b^0(r) \right) / \left(\int_0^{r_w} dr r n_b^0(r) \right)^2. \quad (20)$$

The allowed range of the normalized intensity parameter s_b is $0 \leq s_b < 1$, where the limit $s_b \rightarrow 1$ corresponds to infinitely depressed tune (space-charge-dominated limit).

Typical numerical results obtained from the approximate dispersion relation (18) are presented in Figs. 1 – 5 for the case where $r_w = 3r_b$. Figure 1 shows the normalized

growth rate $(Im\omega)/\omega_f$ plotted versus normalized wavenumber $k_z r_w$ for several values of normalized on-axis beam intensity s_b . Note from Fig. 1 that critical value of $k_z r_w$ for the onset of instability increases as s_b is decreased, and that the maximum normalized growth rate $(Im\omega)_{max}/\omega_f$ is achieved for $s_b = 0.96$ (Fig. 2). In the limit where $k_z r_w \rightarrow \infty$, the growth rate is zero for $s_b < 0.75$. Finite $T_{\parallel b}$ effects introduce a finite bandwidth in $k_z r_w$ for instability, since the modes with large values of $k_z r_w$ are stabilized by Landau damping. Therefore, the stability results in Figs. 2 and 4 – 5 are plotted for moderate value of normalized wavenumber corresponding to $k_z r_w = 8$.

Figure 3 shows the normalized real oscillation frequency $(Re\omega)/\omega_f$ plotted versus normalized wavenumber $k_z r_w$ for $s_b = 0.96$. The high-frequency branches correspond to transverse modes that are present when $k_z r_w = 0$. The low-frequency branches correspond to longitudinal modes that are absent when $k_z r_w = 0$. For $k_z r_w$ greater than some threshold value, the intermediate high-frequency longitudinal mode and the low-frequency transverse mode coalesce and have the same value of real oscillation frequency, $(Re\omega)/\omega_f \approx 0.8$, with growth rate $(Im\omega)/\omega_f$ given by the $s_b = 0.96$ curve in Fig. 1.

The corresponding behavior of the normalized real oscillation frequency $(Re\omega)/\omega_f$ as a function of s_b for fixed $k_z r_w = 8$ is plotted in Fig. 4. For s_b greater than some threshold value, the two branches coalesce. The real oscillation frequency of the resulting branch is a weak function of s_b . The existence of instability thresholds, both for $k_z r_w$ and s_b , is a reflection of the resonant nature of the instability. Indeed, referring to Eq. (18), the beam must be sufficiently intense for the beam plasma frequency to be close to the second harmonic of the effective depressed betatron frequency $\omega_{\beta\perp}$ (Fig. 4). Also, since the longitudinal mode frequency is proportional to the normalized wavenumber $k_z r_w$ (for $k_z r_w \leq 5$) (Fig. 3), the resonant condition is achieved only for sufficiently large values of $k_z r_w$.

The normalized eigenfunction plots of $Re\delta\hat{\phi}(r)$ and $Im\delta\hat{\phi}(r)$ versus r/r_w corresponding to $s_b = 0.96$ and $k_z r_w = 8$ are plotted versus r/r_w in Fig. 5. The real part of the eigenfunction has no zeros, and has a structure similar to the familiar longitudinal mode (L_1) in Ref. [8].

B. Macroscopic Warm-Fluid Description

To remedy the problem arising from an unphysical KV distribution, Strasburg and Davidson [21, 22] employed a warm-fluid model [20] to investigate the stability properties of intense

charged beams with large pressure anisotropy. A waterbag equilibrium and negligible heat-flow were assumed. For $k_z = 0$, the model recovers stable high-frequency ($\omega_n > \sqrt{2}\nu_0$) modes, which are similar to the stable high-frequency T_n modes of a KV beam, whereas the low-frequency unstable T_n modes are absent. For sufficiently large values of $k_z^2 r_b^2$, the anisotropy leads to instability provided the intensity of the beam is sufficiently below the space-charge limit, $\nu/\nu_0 \geq 0.5$. The maximum growth rate $Im\omega/\nu_0 \simeq 0.33$ is achieved for $k_z^2 r_b^2 > 1$ and $0.6 \leq \nu/\nu_0 \leq 0.9$.

The assumption in the warm-fluid description is that the frequencies of the interest are much larger than the resonant frequencies characteristic of the transverse particle motion, so that the contribution from the resonant particles can be neglected. The same assumption allows one to neglect the heat-flow term in the equation for the pressure tensor. Hence, the low-frequency modes ($\omega \approx \nu_0$) are not correctly described by such a warm-fluid model. In the warm-fluid treatment [21, 22], the instability arises as a resonant interaction of the smallest-frequency transverse fluid mode, and the ordinary longitudinal mode at frequency $\omega \approx \nu_0$. At this frequency one can not neglect the resonant interaction with the transverse particle motion, and one must normally employ a kinetic description.

III. DESCRIPTION OF THE NONLINEAR δF SIMULATION CODE

The theoretical model described in Sec. II uses simplified assumptions for the background distribution function. In practical applications, the transverse distribution function may be close to thermal equilibrium with temperature $T_{\perp b}$, and the longitudinal distribution can be described by a drifting Maxwellian distribution with temperature $T_{\parallel b} \ll T_{\perp b}$. This distribution is stable with respect to transverse perturbations [1, 9]. For an arbitrary equilibrium distribution one cannot solve the stability problem analytically and must employ numerical simulation techniques. To investigate stability properties numerically, we use the nonlinear δf method [28] described below, as implemented in the Beam Equilibrium, Stability and Transport (BEST) code [14–16].

In the smooth-focusing approximation, the transverse focusing force is modeled by $\mathbf{F}_{foc} = -\gamma_b m_b \omega_f^2 \mathbf{x}_{\perp}$, where ω_f is the constant focusing frequency associated with applied focusing field, m_b is the particle rest mass, $\gamma_b = (1 - \beta_b^2)^{1/2}$ is the relativistic mass factor, $\beta_b c = const$ is the average axial beam velocity, and c is the speed of light in *vacuo*. The solutions

to the nonlinear Vlasov-Maxwell equations are expressed as $f_b = f_b^0 + \delta f_b$, $\phi = \phi^0 + \delta\phi$ and $A_z = A_z^0 + \delta A_z$, where (f_b^0, ϕ^0, A_z^0) are known equilibrium solutions. The perturbed potentials satisfy the equations [14]

$$\nabla^2 \delta\phi = -4\pi e_b \int d^3p \delta f_b, \quad (21)$$

$$\nabla^2 \delta A_z = -\frac{4\pi}{c} e_b \int d^3p v_z \delta f_b, \quad (22)$$

where e_b is the particle charge, and $\delta f_b(\mathbf{x}, \mathbf{p}, t)$ is given by the weighted Klimontovich representation,

$$\delta f_b = \frac{N_b}{N_{sb}} \sum_{i=1}^{N_{sb}} w_{bi} \delta(\mathbf{x} - \mathbf{x}_{bi}) \delta(\mathbf{p} - \mathbf{p}_{bi}). \quad (23)$$

Here, N_{sb} is total number of beam simulation particles, N_b is total number of actual beam particles, and the weight function is defined by $w_b \equiv \delta f_b / f_b$.

The nonlinear particle simulations are carried out by iteratively advancing the particle motion, including the weights they carry, according to [14]

$$\frac{d\mathbf{x}_{bi}}{dt} = (\gamma_b m_b)^{-1} \mathbf{p}_{bi}, \quad (24)$$

$$\frac{d\mathbf{p}_{bi}}{dt} = -\gamma_b m_b \omega_f^2 \mathbf{x}_{\perp bi} - e_b \left(\nabla \phi - \frac{v_{zbi}}{c} \nabla_{\perp} A_z \right), \quad (25)$$

$$\frac{dw_{bi}}{dt} = -(1 - w_{bi}) \frac{1}{f_{b0}} \frac{\partial f_{b0}}{\partial \mathbf{p}} \cdot \delta \left(\frac{d\mathbf{p}_{bi}}{dt} \right), \quad (26)$$

$$\delta \left(\frac{d\mathbf{p}_{bi}}{dt} \right) = -e_b \left(\nabla \delta\phi - \frac{v_{zbi}}{c} \nabla_{\perp} \delta A_z \right), \quad (27)$$

and updating the fields by solving the perturbed Maxwell's equations with appropriate boundary conditions at the cylindrical, perfectly conducting wall at radius r_w .

The δf approach is fully equivalent to the original nonlinear Vlasov-Maxwell equations, but the noise associated with representation of the background distribution f_b^0 in conventional particle-in-cell (PIC) simulations is removed. In the δf approach, the simulation particles are used to represent only a small part of the entire distribution $\delta f_b = f_b - f_b^0$, and therefore the statistical error in the simulation is proportional to $\epsilon_{\delta f} \sim \delta f_b / \sqrt{N_{sb}}$, whereas the error in PIC simulations is proportional to $\epsilon_{pic} \sim f_b / \sqrt{N_{sb}}$. Therefore, the typical gain in accuracy in δf simulations compared to PIC simulations with the same number of particles is $\epsilon_{\delta f} / \epsilon_{pic} = \bar{w}_{bi}$ [14]. This fact allows much more accurate simulations of the nonlinear dynamics and instability thresholds when $|\bar{w}_{bi}| \ll 1$. When the perturbation δf_b becomes

comparable in magnitude with the background distribution function f_b^0 , then the δf method becomes less accurate than a full PIC simulation. In the present paper, a hybrid combination of the δf and PIC simulation methods is used, where the number density is calculated according to $\delta n_b = [1 - \theta(\bar{w}_{bi})]\delta n_{\delta f} + \theta(\bar{w}_{bi})(n_{pic} - n_0)$, where $\theta(w)$ is a monotonic function of its argument such that $\theta(w \rightarrow 0) \rightarrow 0$ and $\theta(w \rightarrow 1) \rightarrow 1$. Here, $\delta n_{\delta f} = \int d^3p \delta f_b$ and $n_{pic} = \int d^3p f_b$.

In addition, the δf method can be used to study linear stability properties, provided all nonlinear terms in the dynamical equations (25)–(27) are neglected [14–16]. This corresponds to replacing the term $1 - w_{bi}$ with 1 in Eq. (26) for the weights, and moving particles along the trajectories calculated in the unperturbed potentials (ϕ^0, A_z^0) .

The δf method described above has been implemented in the three-dimensional electro-magnetostatic particle-in-cell code (BEST) in cylindrical geometry with a perfectly conducting cylindrical boundary at radius r_w . Maxwell’s equations (21) and (22) are solved using fast Fourier transform techniques (FFT) in the longitudinal and azimuthal directions. The particle positions [Eqs.(24) and (25)] and weights [Eq. (26)] are advanced using a second-order predictor-corrector algorithm. The code is parallelized using Message Passing Interface (MPI) with domain decomposition in the direction of beam propagation. The NetCDF data format is used for large-scale diagnostic and visualization. Typical runs consist of 10^6 simulation particles and are performed on the IBM SP/RS 6000 at NERSC.

IV. SIMULATION RESULTS

Here we present the simulation results for an axially continuous, anisotropic beam in a constant focusing field. For simplicity we perform the simulations in the beam frame. It is assumed that the equilibrium distribution function is bi-Maxwellian and given by equation (1), where \hat{n}_b is the on-axis ($r = 0$) beam density, and $T_{\perp b}$ and $T_{\parallel b}$ are the transverse and longitudinal temperatures of the beam particles. The equilibrium self-field potentials (ϕ_0, A_{z0}) are determined numerically from Maxwell’s equations [14–16]. It is also assumed that the beam is located inside a grounded, cylindrical, perfectly conducting wall at radius $r_w = 3r_b$, where $r_b = [\langle r^2 \rangle]^{1/2}$ is the rms beam radius. Random initial perturbations are introduced to the particle weights, and the beam is propagated from $t = 0$ to $t = 800\omega_f^{-1}$.

The simulations are performed using the nonlinear δf simulation method described in

Sec. III for a wide range of normalized beam intensities ranging from $s_b = 0.1$ to $s_b = 0.95$, and detailed stability properties have been determined for the range of intensity parameters satisfying $s_b \geq 0.5$ assuming axisymmetric perturbations with $\partial/\partial\theta = 0$. Shown in Fig. 6 is the time history of the density perturbation $\delta n_b = \int d^3p \delta f_b$ for normalized beam intensity $s_b = 0.7$. The initial temperature ratio is taken to be $T_{\parallel b}/T_{\perp b} = 0.04$. After the initial exponential growth phase, the instability saturates at a moderately large level with $|\delta n_b^{max}/\hat{n}_b| \simeq 0.05$.

Figures 7 and 8 show plots of the real and imaginary parts of the complex oscillation frequency ω versus normalized axial wavenumber $k_z r_w$. The instability has a finite bandwidth with maximum growth rate $Im\omega/\omega_f \simeq 0.02$ at $k_z r_w = 7.5$. For long wavelengths with $k_z^2 r_w^2 \ll 1$, the dispersion relation is linear with $Re\omega$ proportional to $k_z r_w$. For short wavelengths with $k_z^2 r_w^2 \gg 1$, the transverse beam size is unimportant and $Re\omega \simeq 1.03\omega_f$. The dependence of the maximum growth rate $(Im\omega)_{max}/\omega_f$ on beam intensity s_b is shown in Fig. 9. The maximum growth rate $(Im\omega)_{max}/\omega_f \simeq 0.038$ occurs for $s_b \simeq 0.8$, with no instability in the region $s_b \leq 0.5$.

Figure 10 shows a plot of the real oscillation frequency $Re\omega/\omega_f$ versus normalized beam intensity s_b for the unstable mode. The radial structure of the unstable mode is shown in Fig. 11 for $k_z r_w = 7.5$. Only the real part of the eigenfunction is shown, since $Im\delta\hat{\phi} \approx const \cdot Re\delta\hat{\phi}$ for the weakly unstable mode. The simulation results presented in Figs. 6 – 11 are in good qualitative agreement with the theoretical model presented in Sec. II in terms of the mode structure and real oscillation frequencies (see Figs. 1 – 5). The difference in the absolute value of the growth rate $(Im\omega)_{max}/\omega_f$ in Fig. 2 and Fig. 9, and the existence of the instability cutoff for large values of the normalized wavenumber in Fig. 8, are attributed to the Landau damping associated with the nonzero value of longitudinal temperature $T_{\parallel b}$ in the simulations.

The net change in the longitudinal momentum distribution $\delta F_b(p_z)/\hat{F}_{0b}$ at $\omega_f t = 800$ in the simulation is shown in Fig. 12. Here, $\delta F_b(p_z) = \int d^2p_{\perp} d^3x \delta f_b$ and $\hat{F}_{0b} = \hat{n}_b/(2\pi m_b T_{\parallel b})^{1/2}$. The formation of tails in the axial momentum distribution in Fig. 12 and the consequent saturation of the instability are attributed to quasilinear stabilization due to resonant wave-particle interactions in the tails of the distribution function.

Simulations have also been carried out for different values of temperature anisotropy $T_{\parallel b}/T_{\perp b}$. Plotted in Fig. 13 is the ratio $(T_{\parallel b}^{th})^{1/2} k_z/m_b^{1/2} \omega_f$ versus normalized beam intensity

s_b , where $T_{\parallel b}^{th}$ is the threshold value of longitudinal beam temperature for the onset of instability and k_z is the axial wavenumber.

The saturation mechanism due to resonant wave-particle interactions suggests that the instability is absent if the Landau damping rate due to nonzero thermal spread in the axial direction is greater than the instability growth rate for $T_{\parallel b} = 0$. This implies that $(T_{\parallel b}^{th})^{1/2} k_z / m_b^{1/2} \omega_f \approx \gamma(T_{\parallel b} = 0) / \omega_f$, where $\gamma(T_{\parallel b} = 0)$ is the instability growth rate for $T_{\parallel b} = 0$. In the present simulations, the instability is found to be absent if the ratio of initial axial and transverse temperatures is greater than the threshold value $(T_{\parallel b} / T_{\perp b})^{th} = 0.07$.

Finally, we present simulation results for parameters in the stable regime for $s_b = 0.8$ and $k_z r_w = 3$. The temperature ratio is taken to be $T_{\parallel b} / T_{\perp b} = 0.0025$. Figure 14 shows the frequency spectrum, and Fig. 15 shows the real part of the eigenfunctions for the lowest frequency longitudinal modes. The frequency spectrum in Fig. 14 agrees reasonably well with the theoretical results in Fig. 4. Note from Fig. 14 that the spread in depressed betatron frequency $\omega_{\beta\perp}(H_{\perp})$ results in a finite bandwidth to the frequency curves.

V. CONCLUSIONS

To summarize, in Sec. II we generalized the classical Harris-like instability to the case of an intense charged particle beam with anisotropic temperature ($T_{\parallel b} / T_{\perp b} < 1$) including the important effects of finite transverse geometry and beam space-charge. Using the simplified assumption of negligible spread in depressed betatron frequency, we derived a simple dispersion equation for the lowest-order eigenmodes for the case of extreme temperature anisotropy ($T_{\parallel b} / T_{\perp b} \rightarrow 0$). For sufficiently large values of $k_z^2 r_b^2 \gtrsim 1$, where r_b is the rms beam radius, the analysis of the dispersion equation leads to a strong anisotropy-driven instability provided the normalized beam intensity $s_b = \hat{\omega}_{pb}^2 / 2\omega_f^2$ is sufficiently large. In Sec. IV, the BEST code [14], which implements the nonlinear δf scheme described in Sec. III, was used to investigate the detailed stability properties of intense charged particle beams with large temperature anisotropy ($T_{\parallel b} / T_{\perp b} \ll 1$) assuming axisymmetric perturbations with $\partial/\partial\theta = 0$. The simulation results clearly show that moderately intense beams with $s_b \gtrsim 0.5$ are linearly unstable to short wavelength perturbations with $k_z^2 r_b^2 \gtrsim 1$, provided the ratio of longitudinal and transverse temperatures is smaller than some threshold value. The mode structure, growth rate and conditions for the onset of the instability are qualitatively similar to what is pre-

dicted by the simple theoretical model presented in Sec. II. The main saturation mechanism for the instability is the resonant wave-particle interactions that occur during the formation of tails in the axial momentum distribution. In the nonlinear saturation stage, the total distribution function is still far from equipartitioned, and free energy is available to drive an instability of the hydrodynamic type [21, 22].

VI. ACKNOWLEDGEMENTS

This research was supported by the Department of Energy. It is a pleasure to acknowledge the benefit of useful discussions with Igor Kaganovich, Steve Lund and Wei-li Lee.

VII. REFERENCES

- [1] R. C. Davidson and H. Qin, *Physics of Intense Charged Particle Beams in High Energy Accelerators* (World Scientific, Singapore, 2001), and references therein.
- [2] A. W. Chao, *Physics of Collective Beam Instabilities in High Energy Accelerators* (John Wiley & Sons, Inc., New York, 1993).
- [3] M. Reiser, *Theory and Design of Charged Particle Beams* (John Wiley & Sons, Inc., New York, 1994).
- [4] See, for example, *Proceedings of the 1999 Particle Accelerator Conference* (IEEE, Piscataway, NJ, 1999), pp. 1-3778.
- [5] See, for example, Proceedings of the 1999 International Heavy Ion Fusion Symposium, Nuclear Instruments and Methods in Physics Research **A**, pp. 1-674 (2001).
- [6] I. M. Kapchinskij and V. V. Vladimirskij, in *Proceedings of the International Conference on High Energy Accelerators and Instrumentation* (CERN Scientific Information Service, Geneva, 1959), p.274.
- [7] R. L. Gluckstern, in *Proceedings of the 1970 Proton Linear Accelerator Conference*, Batavia, IL, edited by M. R. Tracy (National Accelerator Laboratory, Batavia, IL, 1971), p. 811.
- [8] T. -S. Wang and L. Smith, *Particle Accelerators* **12**, 247 (1982).
- [9] R. C. Davidson, *Phys. Rev. Lett.* **81**, 991 (1998).
- [10] R. C. Davidson and H. Qin, *Physical Review Special Topics on Accelerators and Beams* **2**, 114401 (1999).
- [11] W. W. Lee, Q. Qian, and R. C. Davidson, *Physics Letters* **A230**, 347 (1997).
- [12] Q. Qian, W. W. Lee, and R. C. Davidson, *Phys. Plasmas* **4**, 1915 (1997).
- [13] P. H. Stoltz, R. C. Davidson, and W. W. Lee, *Phys. Plasmas* **6**, 298 (1999).
- [14] H. Qin, R. C. Davidson and W. W. Lee, *Physical Review Special Topics on Accelerators and Beams* **3**, 084401 (2000); **3**, 109901 (2000).
- [15] H. Qin, R. C. Davidson, W. W. Lee and E. A. Startsev, *Proceedings of the 2001 Particle Accelerator Conference* (IEEE, Piscataway, NJ, 2001), p. 693.
- [16] E. A. Startsev, R. C. Davidson, W. W. Lee and H. Qin, *Proceedings of the 2001 Particle*

- Accelerator Conference* (IEEE, Piscataway, NJ, 2001), p. 3081.
- [17] I. Hofmann, L. J. Laslett, L. Smith and I. Haber, *Particle Accelerators* **13**, 145 (1983).
 - [18] S. M. Lund, J. J. Barnard, G. D. Craig, A. Friedman, D. P. Grote, T. S. Sangster, W. M. Sharp, S. Eylon, T. T. Fessenden, E. Henestroza, S. Yu, and I. Haber, *Nuclear Instruments and Methods in Physics Research A* **415**, 345 (1998).
 - [19] A. Friedman, J. J. Barnard, D. P. Grote, and I. Haber, *Nuclear Instruments and Methods in Physics Research A* **415**, 455 (1998).
 - [20] S. M. Lund and R. C. Davidson, *Phys. Plasmas* **5**, 3028 (1998).
 - [21] S. Strasburg and R. C. Davidson, *Physics Letters* **A269**, 40 (2000).
 - [22] R. C. Davidson and S. Strasburg, *Phys. Plasmas* **7**, 2657 (2000).
 - [23] I. Hofmann, *Phys. Rev.* **E57**, 4713 (1998).
 - [24] E. G. Harris, *Phys. Rev. Lett.* **2**, 34 (1959).
 - [25] A. B. Mikhailovskii, *Theory of Plasma Instabilities, Volume 1* (Consultants Bureau, New York, 1974), pp. 183-197.
 - [26] A. Friedman, private communication (2001).
 - [27] I. Haber, private communication (2001).
 - [28] S. E. Parker and W. W. Lee, *Phys. Fluids B* **5**, 77 (1993).
 - [29] A. Friedman, D. A. Callahan, D. P. Grote, and A. B. Langdon, *Bull. Am. Phys. Soc.* **35**, 2121 (1990).
 - [30] A. Friedman, R. O. Bangerter, D. A. Callahan, D. P. Grote, and A. B. Langdon, *Proceedings of the 2nd European Particle Accelerator Conference*, 1699 (1990), edited by P. A. Martin, Vol 2.
 - [31] A. Friedman, D. P. Grote and I. Haber, *Phys. Fluids B* **4**, 2203 (1992).
 - [32] S. M. Lund, D. A. Callahan, A. Friedman, D. P. Grote, I. Haber, and T. F. Wang, *Proceedings of XIX International Linear Accelerator Conference* Chicago, 1998, edited by C. E. Eyberger, R. C. Pardo and M. M. White (Argonne National Laboratory, Argonne, Illinois, 1998). p.372.
 - [33] I. Haber, A. Friedman, D. P. Grote, S. M. Lund, and R. A. Kishek, *Phys. Plasma* **6**, 2254 (1999).

VIII. FIGURE CAPTIONS

Fig.1: Plot of $(Im\omega)/\omega_f$ versus $k_z r_w$ obtained from Eq. (18) for $r_w = 3r_b$ and several values of normalized beam intensity s_b defined in Eq. (20).

Fig.2: Plot of $(Im\omega)/\omega_f$ versus normalized beam intensity s_b obtained from Eq. (18) for $r_w = 3r_b$ and $k_z r_w = 8$.

Fig.3: Plot of $(Re\omega)/\omega_f$ versus $k_z r_w$ obtained from Eq. (18) for $r_w = 3r_b$ and $s_b = 0.96$.

Fig.4: Plot of $(Re\omega)/\omega_f$ versus normalized beam intensity s_b obtained from Eq. (18) for $r_w = 3r_b$ and $k_z r_w = 8$.

Fig.5: Radial mode structure of the unstable eigenfunction for $r_w = 3r_b$ and $k_z r_w = 8$ and $s_b = 0.96$.

Fig.6: Time history of the density perturbation $\delta n_{max}/\hat{n}_b$ for normalized beam intensity $s_b = 0.7$ at fixed z and $r = 0.2r_b$.

Fig.7: Normalized eigenfrequency $Re\omega/\omega_f$ plotted versus $k_z r_w$ for $s_b = 0.7$ and $r_w = 3r_b$, and initial $T_{\parallel b}/T_{\perp b} = 0.04$.

Fig.8: Normalized growth rate $Im\omega/\omega_f$ plotted versus $k_z r_w$ for $s_b = 0.7$ and $r_w = 3r_b$, and initial $T_{\parallel b}/T_{\perp b} = 0.04$.

Fig.9: Plot of $(Im\omega)_{max}/\omega_f$ versus normalized beam intensity s_b for $r_w = 3r_b$, and initial $T_{\parallel b}/T_{\perp b} = 0.04$.

Fig.10: Plot of $(Re\omega)/\omega_f$ versus normalized beam intensity s_b for $k_z r_w = 7.5$ and $r_w = 3r_b$, and initial $T_{\parallel b}/T_{\perp b} = 0.04$.

Fig.11: Radial mode structure of the unstable eigenfunction for $k_z r_w = 7.5$, $s_b = 0.7$ and $r_w = 3r_b$, and initial $T_{\parallel b}/T_{\perp b} = 0.04$.

Fig.12: Perturbed axial momentum distribution $\delta F_b(p_z)/\hat{F}_{0b}$ at time $t = 800\omega_f^{-1}$, for normalized beam intensity $s_b = 0.7$ and $r_w = 3r_b$, and initial $T_{\parallel b}/T_{\perp b} = 0.04$.

Fig.13: Ratio $(T_{\parallel b}^{th})^{1/2}k_z/m_b^{1/2}\omega_f$ plotted versus normalized beam intensity s_b for $r_w = 3r_b$.

Fig.14: Frequency spectrum of stable oscillations for $k_z r_w = 3$, $s_b = 0.8$ and $r_w = 3r_b$.

Fig.15: Radial mode structure of the stable eigenfunction for $k_z r_w = 3$, $s_b = 0.8$ and $r_w = 3r_b$.

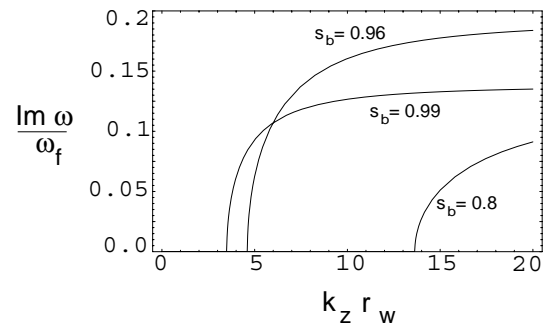


FIG. 1:

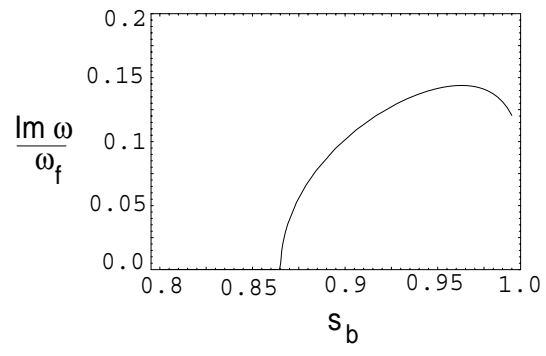


FIG. 2:

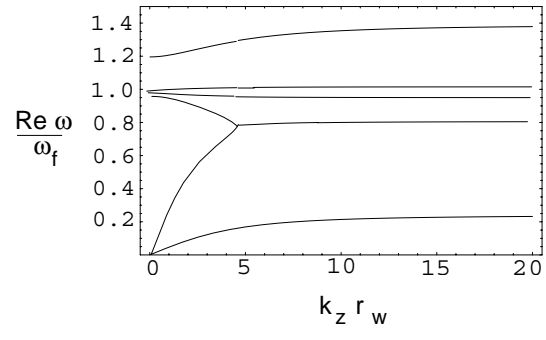


FIG. 3:

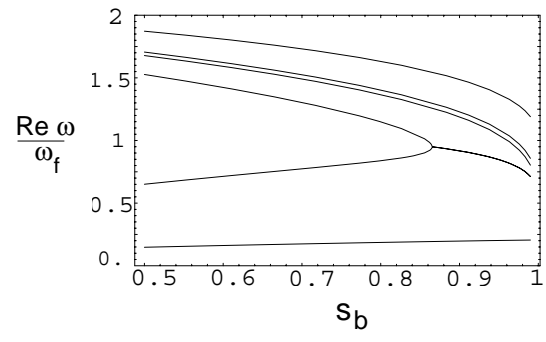


FIG. 4:

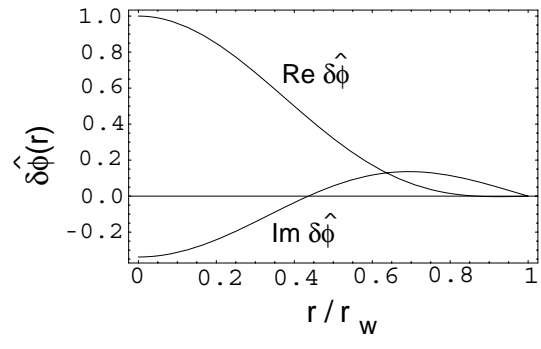


FIG. 5:

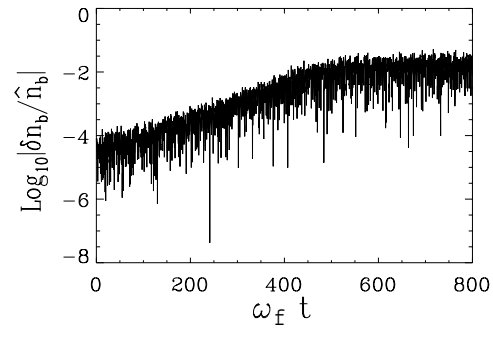


FIG. 6:

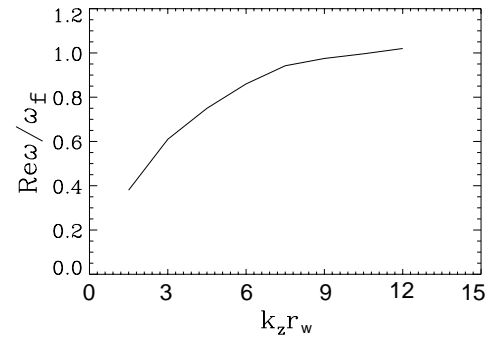


FIG. 7:

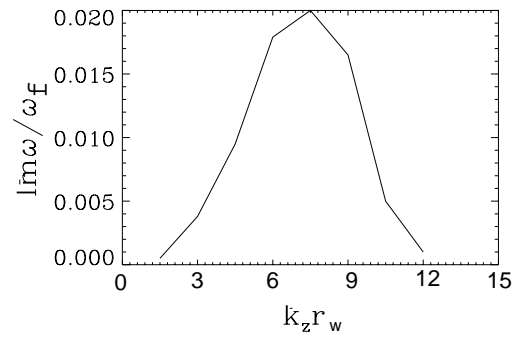


FIG. 8:

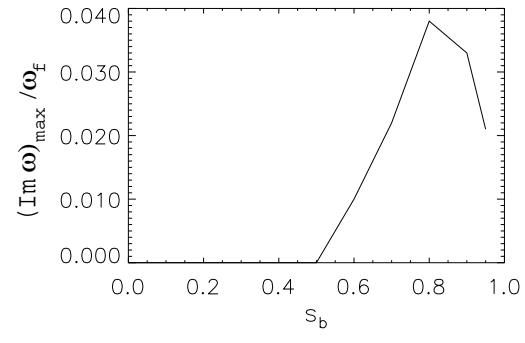


FIG. 9:

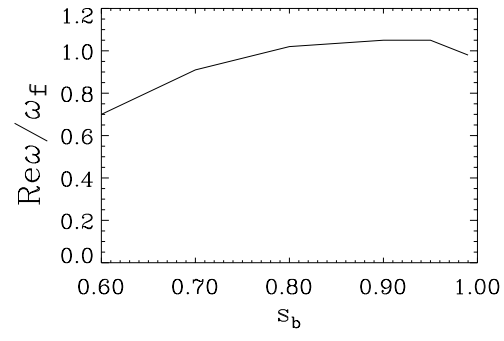


FIG. 10:

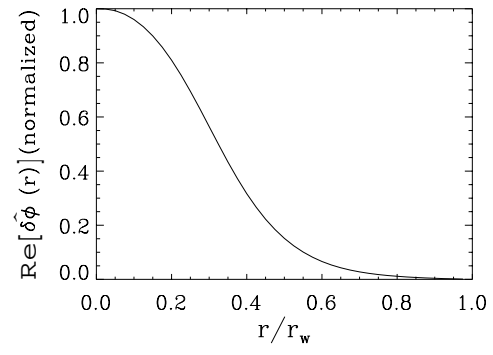


FIG. 11:

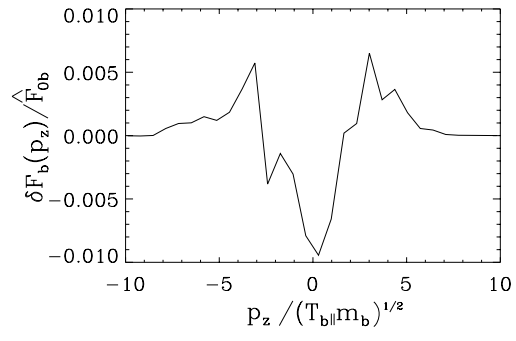


FIG. 12:

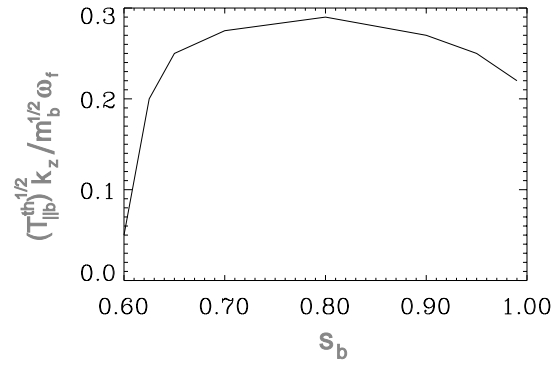


FIG. 13:

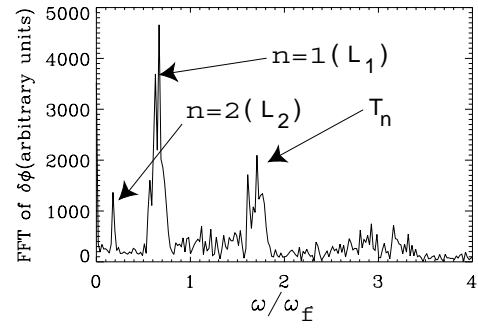


FIG. 14:

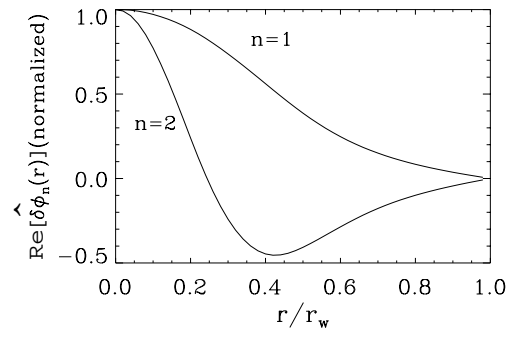


FIG. 15:

External Distribution

Plasma Research Laboratory, Australian National University, Australia
Professor I.R. Jones, Flinders University, Australia
Professor João Canalle, Instituto de Fisica DEQ/IF - UERJ, Brazil
Mr. Gerson O. Ludwig, Instituto Nacional de Pesquisas, Brazil
Dr. P.H. Sakanaka, Instituto Fisica, Brazil
The Librarian, Culham Laboratory, England
Library, R61, Rutherford Appleton Laboratory, England
Mrs. S.A. Hutchinson, JET Library, England
Professor M.N. Bussac, Ecole Polytechnique, France
Librarian, Max-Planck-Institut für Plasmaphysik, Germany
Jolan Moldvai, Reports Library, MTA KFKI-ATKI, Hungary
Dr. P. Kaw, Institute for Plasma Research, India
Ms. P.J. Pathak, Librarian, Institute for Plasma Research, India
Ms. Clelia De Palo, Associazione EURATOM-ENEA, Italy
Dr. G. Grosso, Instituto di Fisica del Plasma, Italy
Librarian, Naka Fusion Research Establishment, JAERI, Japan
Library, Plasma Physics Laboratory, Kyoto University, Japan
Research Information Center, National Institute for Fusion Science, Japan
Dr. O. Mitarai, Kyushu Tokai University, Japan
Library, Academia Sinica, Institute of Plasma Physics, People's Republic of China
Shih-Tung Tsai, Institute of Physics, Chinese Academy of Sciences, People's Republic of China
Dr. S. Mirnov, TRINITI, Troitsk, Russian Federation, Russia
Dr. V.S. Strelkov, Kurchatov Institute, Russian Federation, Russia
Professor Peter Lukac, Katedra Fyziky Plazmy MFF UK, Mlynska dolina F-2, Komenskeho
Univerzita, SK-842 15 Bratislava, Slovakia
Dr. G.S. Lee, Korea Basic Science Institute, South Korea
Mr. Dennis Bruggink, Fusion Library, University of Wisconsin, USA
Institute for Plasma Research, University of Maryland, USA
Librarian, Fusion Energy Division, Oak Ridge National Laboratory, USA
Librarian, Institute of Fusion Studies, University of Texas, USA
Librarian, Magnetic Fusion Program, Lawrence Livermore National Laboratory, USA
Library, General Atomics, USA
Plasma Physics Group, Fusion Energy Research Program, University of California at San
Diego, USA
Plasma Physics Library, Columbia University, USA
Alkesh Punjabi, Center for Fusion Research and Training, Hampton University, USA
Dr. W.M. Stacey, Fusion Research Center, Georgia Institute of Technology, USA
Dr. John Willis, U.S. Department of Energy, Office of Fusion Energy Sciences, USA
Mr. Paul H. Wright, Indianapolis, Indiana, USA

The Princeton Plasma Physics Laboratory is operated
by Princeton University under contract
with the U.S. Department of Energy.

Information Services
Princeton Plasma Physics Laboratory
P.O. Box 451
Princeton, NJ 08543

Phone: 609-243-2750
Fax: 609-243-2751
e-mail: pppl_info@pppl.gov
Internet Address: <http://www.pppl.gov>